Proceedings of the
5th ASME/JSME Joint Thermal Engineering Conference
March 15-19, 1999, San Diego, California

AJTE99-6385

NUMERICAL ANALYSIS OF TURBULENT STRUCTURE THROUGH A CIRCULAR-TO-RECTANGULAR TRANSITION DUCT

Hitoshi SUGIYAMA
Energy and Environmental Science
Utsunomiya University
7-1-2 Youtou Utsunomiya 321-8585
Japan
Email: sugiyama@cc.utsunomiya-u.ac.jp

Mitsunobu AKIYAMA
Department of Mechanical Systems
Utsunomiya University
7-1-2 Youtou Utsunomiya 321-8585
Japan
Email: akiyama@cc.utsunomiya-u.ac.jp

Daisuke HITOMI
Graduate School of Engineering
Utsunomiya University
7-1-2 Youtou Utsunomiya 321-8585
Japan
Email: hitomi@mech.utsunomiya-u.ac.jp

Keywords: Numerical analysis, Turbulent flow, Algebraic Reynolds stress model, Transition duct

ABSTRACT

Numerical analysis is used to investigate three dimensional turbulent structure and fluid flow behavior in a circular-to-rectangular transition duct. The CR transition duct configuration for the present calculation has been shown in Fig. A-1. In the calculation, an algebraic Reynolds stress model together with a boundary-fitted coordinate system is applied to a circular-to-rectangular duct in order to solve anisotropic turbulent flow precisely. The calculated results are compared with the experimental results to examine the validity of the present method. The compared quantities include the streamwise mean-velocity, transverse mean velocity vectors, mean longitudinal vorticity and components of the Reynolds stress tensor. For example, the comparison of streamwise velocity at $X_1/R = 4.0$, where is in the midregion of transition, is displayed in Fig. A-2. The generation of the low velocity observed near the side wall is indicative of the longitudinal vortex pair that is formed as a result of the secondary motion. In comparison with the experimental results, it is found that the present method well predicts a secondary flow pattern which develops into a discrete vortex pair along the duct sidewalls. The vortex pair significantly distorts both the mean flow and turbulence field. As for the comparison of several Reynolds stress components, although the agreement are not perfect in detail, main features are reproduced by the present method. These calculated results suggest that an algebraic Reynolds stress model is useful for this complicated turbulent flow.

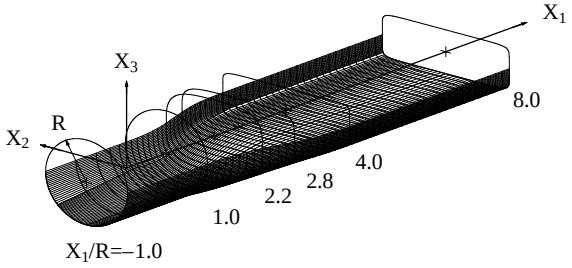

Figure A-1. Circular-to-rectangular transition duct

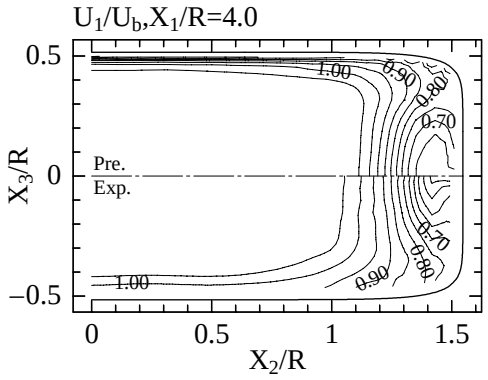

Figure A-2. Comparison of streamwise mean-velocity contours

INTRODUCTION

The duct which has changing cross sectional shape in the streamwise direction is refered to as transition duct. Although transition ducts are commonly used in various engineering fields, one particular transition duct that is currently of interest is the circular-to-rectangular (CR) duct. Nonaxisymmetric engine exhaust nozzles, usually of rectangular cross section, are being developed in order to improve the performance of aircraft.

From the review of literature revealed that there were only a small experimental database for turbulent flow through CR transition duct, Davis and Gessner(1992) measured the turbulent structure contained the six Reynolds stress components in detail. Their experimental results are intended not only to provide insight into the physics of the flow, but also to serve as a basis for testing turbulent models applicable to this type of flow situation.

In numerical analysis, Lien and Leschziner(1993) presented numerical results of CR transition duct, being compared with the experimental data measured by Davis and Gessner(1992) by using high-Reynolds and low-Reynolds numbers k-ε turbulent model. Sotiropoulos and Patel(1994) have employed the near wall, full Reynolds-stress closure to calculate the flow through the CR duct of Davis and Gessner(1992). As for the comparison of Reynolds stresses, they showed that calculated results are in good agreement with the measurements at the end of transition region except for downstream straight duct.

Considering from the review of literature as mentioned above, it is found that several numerical analyses have been performed for the turbulent flow of CR duct database measured by Davis and Gessner(1992) in order to confirm the various kinds of turbulent models. From this standpoint of validation of turbulent model, the main object of this research is to predict the turbulent structure of CR transition duct of Davis and Gessner(1992) by using an algebraic Reynolds stress model. The boundary-fitted coordinate system is adopted in this study as the method of coordinate transformation. The calculated results are compared with the experimental data in order to examine the validity of the present method and to provide insight into the physics of flow for CR transition duct.

NOMENCLATURE

D : inlet pipe diameter
k : kinetic energy of turbulence
L : length scale of turbulence
P_k : production term of turbulent energy equation
R : inlet pipe radius
R_e : Reynolds number= $U_b D/\nu$
$\overline{u_i u_j}$: Reynolds stress components

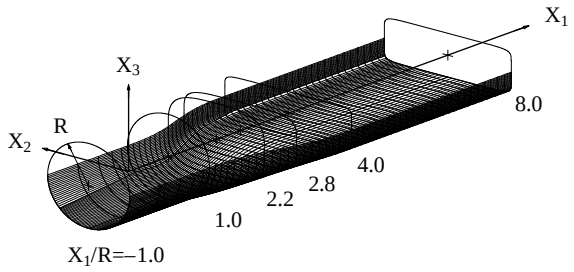

Figure 1. Circular-to-rectangular transition duct and definition of coordinate system

U_i : mean velocity components
U_b : bulk velocity
X_i : primary cartesian coordinate system
ε : dissipation rate of turbulent kinetic energy
ν : kinematic viscosity
π_{ij} : pressure-strain correlation
ρ : density

TECHNIQUE OF ANALYSIS

Subject of numerical analysis

Figure 1 shows a schematic diagram of the experimental apparatus and the coordinate system set in CR transition duct. The origin of the coordinate system lies midway between $X_1/R = -1.0$ and 1.0, where R is pipe radius. The CR transition duct has an exit aspect ratio of 3.0 and a transition length of 4.5 times the inlet diameters(inlet diameter $D = 20.42$ cm) which changes in cross-sectional shape occur. The cross-sectional configuration is defined by the equation of a superellipse,namely:

$$\left(\frac{X_2}{a}\right)^{\eta} + \left(\frac{X_3}{b}\right)^{\eta} = 1 \qquad (1)$$

where a and b are the semi-major and semi-minor axes of the superellipse, respectively and a, b and η are functions of the streamwise coordinate X_1 which are described by Davis(1991) in detail. The cross-sectional area begins to increase at the start of transition to a maximum of 15 % above the inlet cross-sectional area, occurring approximately at the mid-point of transition. From there the area smoothly decreases until the end of transition where the cross-sectional area is equal to the inlet cross- sectional area.

From the 20:1 contraction, the flow enters a 20.42 cm diameter straight pipe of 184 cm in length. Downstream of the transition duct, the flow enters a rectangular duct of 89 cm in length.

In the experiment, Reynolds number evaluated with an axial bulk velocity U_b and pipe diameter D was kept at $R_e = 3.9 \times 10^5$. Mean flow and turbulence data were obtained by means of pressure probe and hot-wire instrumentation. The turbulence measurement was carried out especially for the cross sections at $X_1/R = 4.0$ and 8.0.

Algebraic Reynolds stress model

The set of differential equations governing the transport of the Reynolds stresses is derived from the Navier- Stokes equation as follows:

$$\frac{D\overline{u_i u_j}}{Dt} = -(\overline{u_i u_k}\frac{\partial U_j}{\partial X_k} + \overline{u_j u_k}\frac{\partial U_i}{\partial X_k}) - \frac{\partial}{\partial X_k}[(\overline{u_i u_j u_k} - \nu\frac{\partial \overline{u_i u_j}}{\partial X_k} + \overline{\frac{p}{\rho}(\delta_{jk}u_i + \delta_{ik}u_j)}] + \overline{\frac{p}{\rho}(\frac{\partial u_i}{\partial X_j} + \frac{\partial u_j}{\partial X_i})} - 2\nu\overline{\frac{\partial u_i}{\partial X_k}\frac{\partial u_j}{\partial X_k}} \quad (2)$$

As for the modeling of the convective term and of the diffusion term,the approximation by Rodi(1976) was employed. With Rodi's approximation, these terms expressed in a differential form for Reynolds stress component can be transformed into the algebraic equation. In the transport equations of the Reynolds stresses, a particularly problematic task is the modeling of the pressure-strain correlation term which is also defined redistribution term. The slow term $\pi_{ij,1}$(Eq.(3).), rapid term $\pi_{ij,2}$(Eq.(4).) and wall reflection term $\pi_{ij,w}$(Eq.(5). $\sim$ (7).) involved in the pressure-strain term are modelled as follows in this research:

$$\pi_{ij,1} = -C_1\frac{\varepsilon}{k}\left(\overline{u_i u_j} - \frac{2}{3}k\delta_{ij}\right) \quad (3)$$

$$\pi_{ij,2} = -\frac{C_2+8}{11}\left(P_{ij} - \frac{2}{3}P_k\delta_{ij}\right) + \zeta k\left(\frac{\partial U_i}{\partial X_j} + \frac{\partial U_j}{\partial X_i}\right) - \frac{8C_2-2}{11}\left(D_{ij} - \frac{2}{3}P_k\delta_{ij}\right) \quad (4)$$

Table 1. Constants in the pressure-strain correlation terms

C_1^*	C_2^*	ζ^*	C_1'	C_2'	ζ'
1.4	0.44	-0.16	-0.35	0.12	-0.1

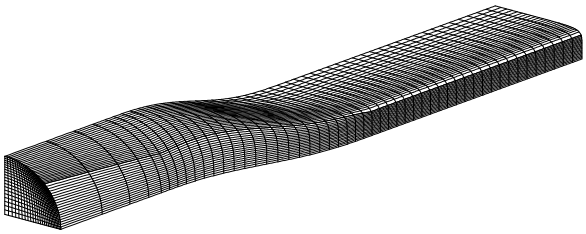

Figure 2. Computational mesh

$$C_1 = C_1^* + C_1' f\left(\frac{L}{X_w}\right) \quad (5)$$

$$C_2 = C_2^* + C_2' f\left(\frac{L}{X_w}\right) \quad (6)$$

$$\zeta = \zeta^* + \zeta' f\left(\frac{L}{X_w}\right) \quad (7)$$

where

$$P_{ij} = -\overline{u_i u_k}\frac{\partial U_j}{\partial X_k} - \overline{u_j u_k}\frac{\partial U_i}{\partial X_k} \quad (8)$$

$$D_{ij} = -\overline{u_i u_k}\frac{\partial U_k}{\partial X_j} - \overline{u_j u_k}\frac{\partial U_k}{\partial X_i} \quad (9)$$

$$P_k = -\overline{u_k u_l}\frac{\partial U_k}{\partial X_l} \quad (10)$$

$$f\left(\frac{L}{X_w}\right) = \frac{C_\mu^{\frac{3}{4}}}{\kappa}\frac{k^{\frac{3}{2}}}{\varepsilon}\frac{1}{X_w} \quad (11)$$

The constants used in this analysis are summarized in Table 1. In the modeling of $\pi_{ij,2}$, we made use of the forth-order tensor presented by Launder, Reece and Rodi(1975). Moreover, kinematic constraints presented by Gessner and Eppich(1981) are adopted in this research. Sugiyama et al.(1993) described the derivation of pressure-strain and its constants in detail. Equation (11). is defined as a function of the dimensionless wall distance. It expresses the influence of the wall and takes the value 1 in its vicinity, approaching 0 in with the increasing distance of it. X_w expresses the distance from the wall and L defines the length scale of turbulence.

Boundary-fitted coordinate system (BFC) was adopted as the coordinate transformation in this research. The transformation of the governing equations to the calculation level is accomplished according to following mathematical definitions:

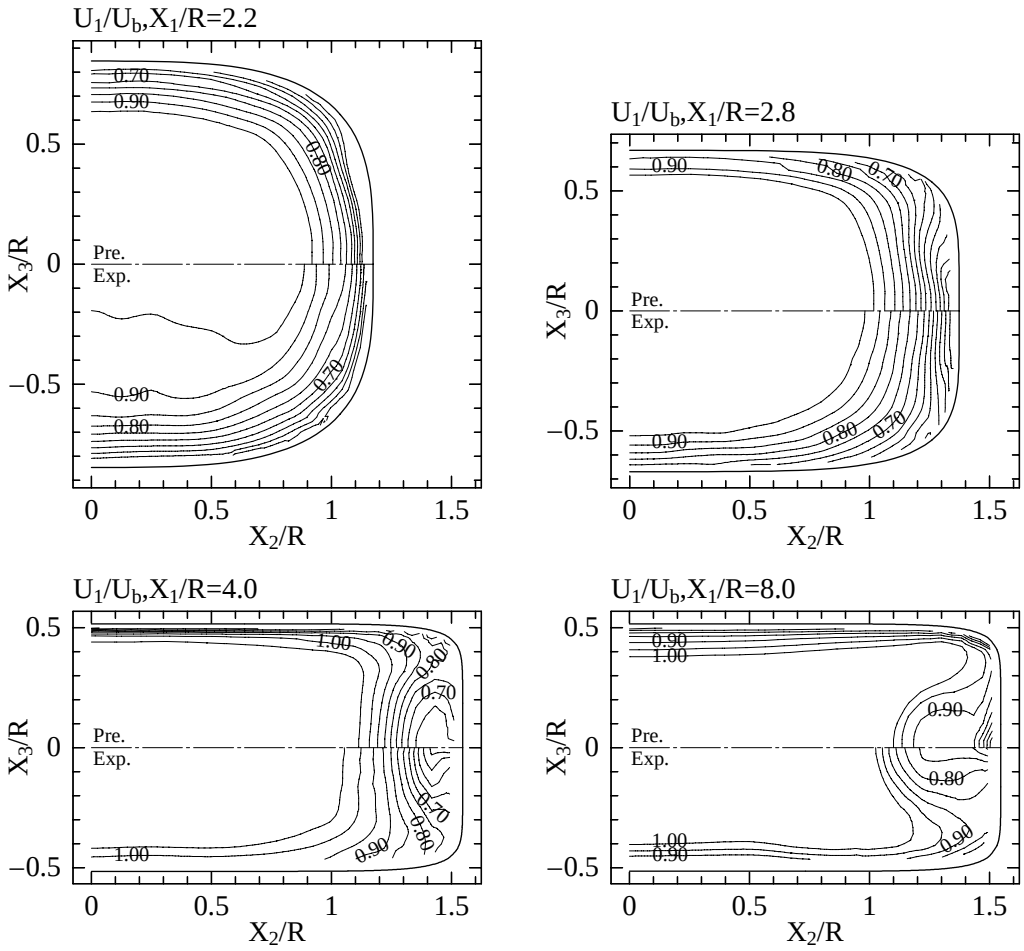

Figure 3. Comparison of streamwise mean-velocity contours

$$\frac{\partial}{\partial X_i} = \frac{\partial \xi}{\partial X_i}\frac{\partial}{\partial \xi} + \frac{\partial \eta}{\partial X_i}\frac{\partial}{\partial \eta} + \frac{\partial \zeta}{\partial X_i}\frac{\partial}{\partial \zeta} \qquad (12)$$

The procedure of the transformation of the governing equations has been described in detail by the author's other report(1995). The governing equations are discretized by employing finite differential method with non-staggered computational grids. The QUICK(Quadratic Interpolation for Convective Kinematics) approximation of Leonard(1979) is used for discretizing convective transport term and the other terms are discretized with central-difference scheme. In numerical solution, implicit method is adopted and successive over relaxation method is utilized as a solution of the algebraic equations.

Numerical analysis

We set computational domain on a quarter region of the whole cross section from the symmetry of CR transition duct. Adding to this, upstream entry length of $30D$ with circular cross section and a downstream tangent of $30D$ with rectangular cross section were used in this calculation. Therefore, total length of transition duct became $64.5D$. Reynolds number of this calculation is equal to one of the experiment. As for the inlet condition of the straight pipe, the value of $k = U_b^2 \times 10^{-5}$ and $\varepsilon = k^{3/2}/D$ were adopted by assuming small fluctuating velocity at the duct inlet. The consistence of the universal velocity distribution in the vicinity of the wall and also the supposition of the local equilibrium lead to the utilization of the law of the wall function as the boundary conditions for k and ε equations. The present turbulent model is classified as a high Reynolds number model, so that we made use of wall

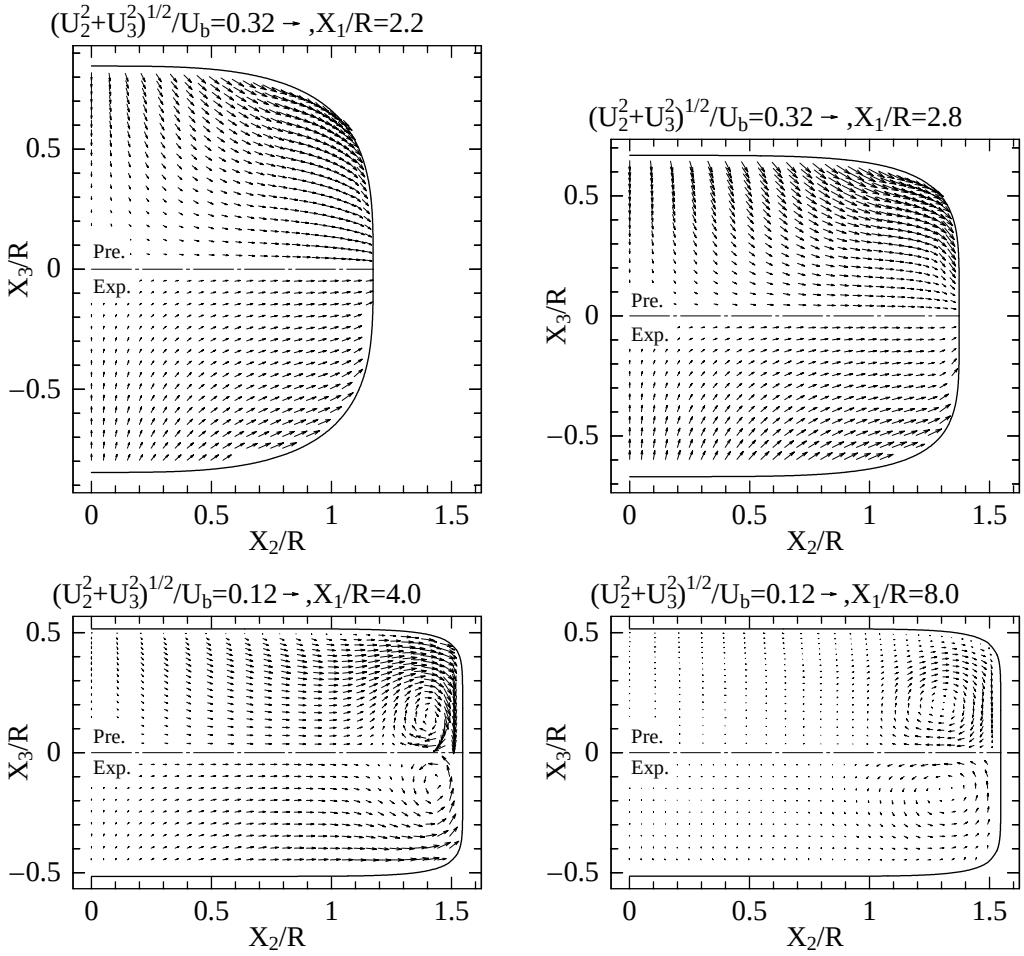

Figure 4. Comparison of transverse mean-velocity vectors

function method.

Figure 2 shows the arrangement of the calculation mesh over the CR transition duct. Numerical grids are located finely where the variation of physical parameters are observed. Calculation have been carried out on a numerical grid with 130 nodes in the streamwise and with 25×20 in the quarter region of total cross-section.

RESULTS AND DISCUSSION

Mean flow results

Although the experimental results are shown in a half cross-section, comparisons between both results are displayed in a quarter cross-section judging from the symmetrical results of the experimental data. Streamwise mean flow is compared at X_1/R = 2.2, 2.8, 4.0 and 8.0 as shown in Fig. 3. Reference coordinates applicable to these data are shown in Fig. 1. It is found from both results that streamwise velocity contours follow the cross-sectional shape at $X_1/R = 2.2$ and 2.8 and a distortion of contours is seen to develop in the vicinity of the sidewall at $X_1/R = 4.0$ and 8.0. The numerical results can reproduce these characteristic features. Moreover, it is pointed out as a discrepancy between both results that the present method is not able to predict well a distorted contours in the vicinity of the sidewall at $X_1/R = 8.0$. The distortion of streamwise velocity is caused by a secondary flow which develops into a separated vortex pair along the duct sidewalls.

Figure 4 shows the comparison of secondary flow at the same cross-section of streamwise velocity. The secondary flow arises as a result of lateral skewing of the near-wall flow in the vicinity of the sidewall induced by transverse pressure gradients related with wall curvature. Therefore,

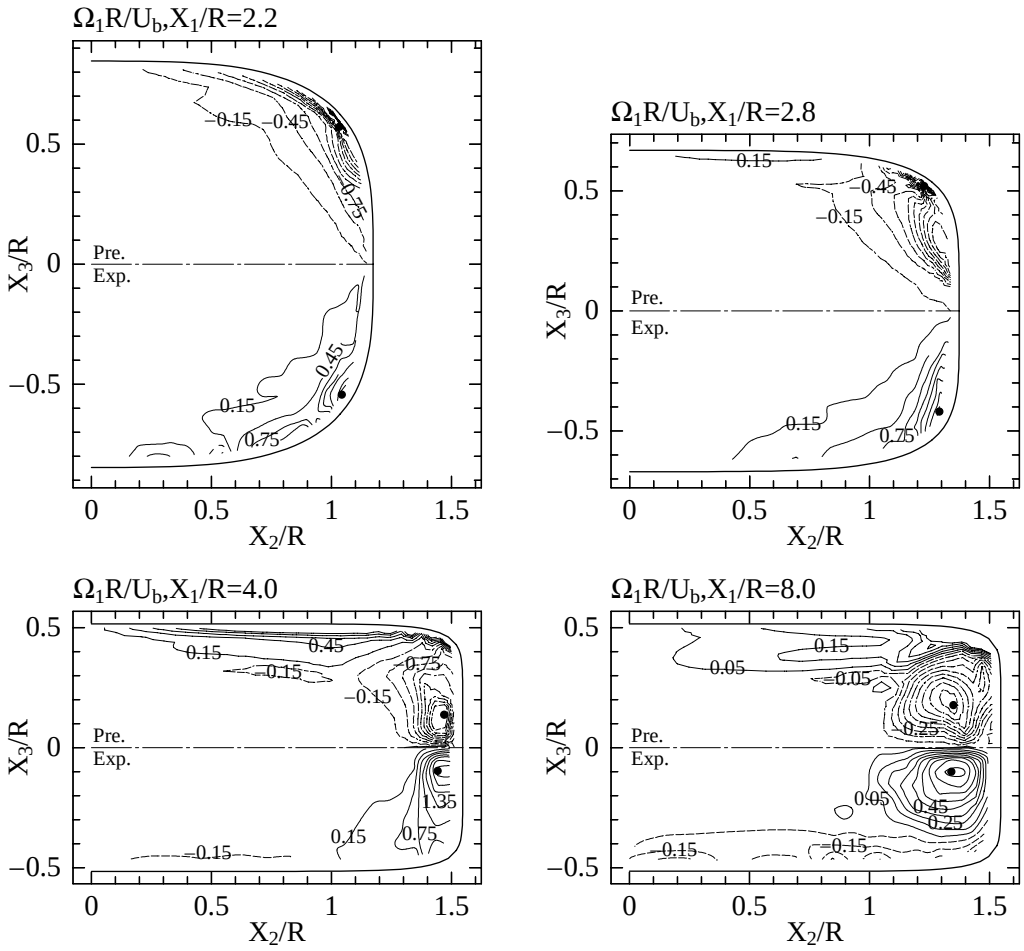

Figure 5. Comparison of mean longitudinal vorticity

the secondary flow of this CR transition duct is defined as the secondary flow of the first kind. At $X_1/R = 2.2$ and 2.8, the secondary currents proceed from the center region of the duct toward the sidewall. As the flow develops, the vortices have grown to the lateral extent are more circular and are centered further away from the sidewall. Between $X_1/R = 4.0$ and 8.0, the strength of the secondary flow decays gradually. These characteristic features are observed in both results. In the light of the experimental results, the present method well predicts the secondary flow vectors. Though Lien and Leschziner(1993) also presented secondary vectors, the discrepancy between their calculations and experimental results was observed in the vicinity of the sidewall at $X_1/R = 4.0$ and 8.0.

The secondary motion is displayed through contours of the mean longitudinal vorticity ($\Omega_1 = \partial U_3/\partial X_2 - \partial U_2/\partial X_3$) constructed by differentiation of the transverse mean-velocity components. The experimental and computed contours at the four sections are shown in Fig. 5. In this figure, the locations of the points of the maximum longitudinal vorticity are indicated by dots. The calculated results are successful in realizing the various features exhibited by the measurements. For instance, the location of maximum vorticity is predicted as well as the calculated results of Sotiropoulos and Patel(1994).

Turbulence results

The comparison of streamwise normal stress $\overline{u_1^2}$ is shown in Fig. 6. As a common feature in these results, distorted contours induced by the secondary flow exist near the sidewall. These contours are distorted more clearly at $X_1/R = 8.0$ than those of $X_1/R = 4.0$. Compared with the experimental data about its value, it is found that the present method has a tendency to overestimate the value of

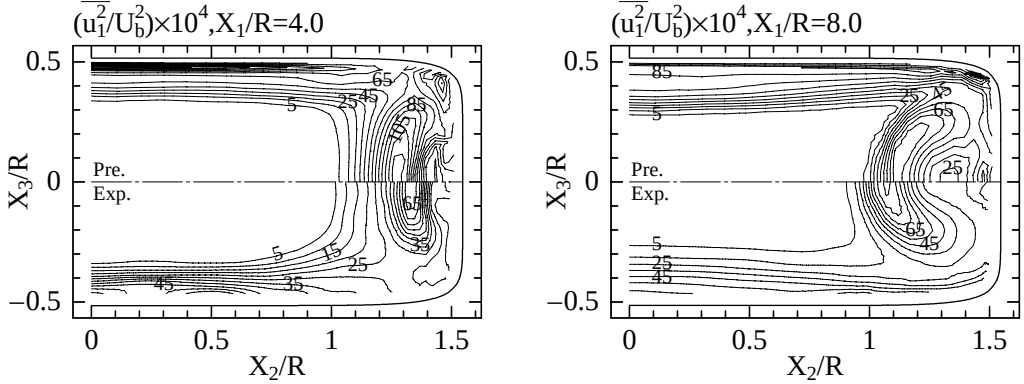

Figure 6. Comparison of normal stress $\overline{u_1^2}$

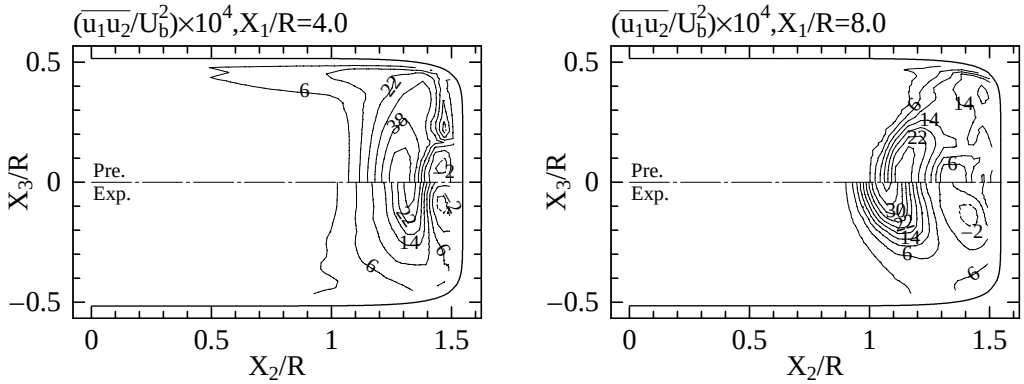

Figure 7. Comparison of shear stress $\overline{u_1u_2}$

these normal stresses.

The comparison of shear stress $\overline{u_1u_2}$, and $\overline{u_1u_3}$ are illustrated in Figs. 7 and 8, respectively. Negative contour levels are represented by dashed lines. As shown in Fig. 7, the primary shear stress $\overline{u_1u_2}$ is observed to be positive everywhere except for the small region in the vicinity of the vortex cores at $X_1/R = 4.0$ in both results. These regions of negative stress result from the positive mean rate-of-strain($\partial U_1/\partial X_2$) induced by distorted streamwise contours as shown in Fig. 3. At downstream $X_1/R = 8.0$ for calculated results, the negative region disappears in the vicinity of sidewall as a result of secondary flow does not cause a bulging of streamwise velocity contours along the $X_3/R = 0$ midplane. Except for this discrepancy, the calculated results of $\overline{u_1u_2}$ are in good agreement with the experimental data.

The distributions of primary shear stress $\overline{u_1u_3}$ show the symmetrical contours with different sign with respect to $X_3/R = 0$ midplane as displayed in Fig. 8. It is found as a characteristic feature in both results that two peaks of absolute value exist near the sidewall. The present method reproduce the experimental distribution not only qualitatively but also quantitatively.

CONCLUSIONS

Numerical analysis has been carried out for developing turbulent flow in a circular-to-rectangular transition duct having the same inlet and outlet cross-section areas, an overall length-to-diameter ratio of 4.5, and aspect ratio of 3.0 at the exit plane. In order to precisely predict anisotropic turbulence of the CR transition duct, an algebraic Reynolds stress model coupled with boundary-fitted coordinate system was adopted in this study. The following conclusions can be drawn from the present study.

With regard to the streamwise velocity contours, the present method can reproduce the characteristic features displaying distorted contours as the flow develops except

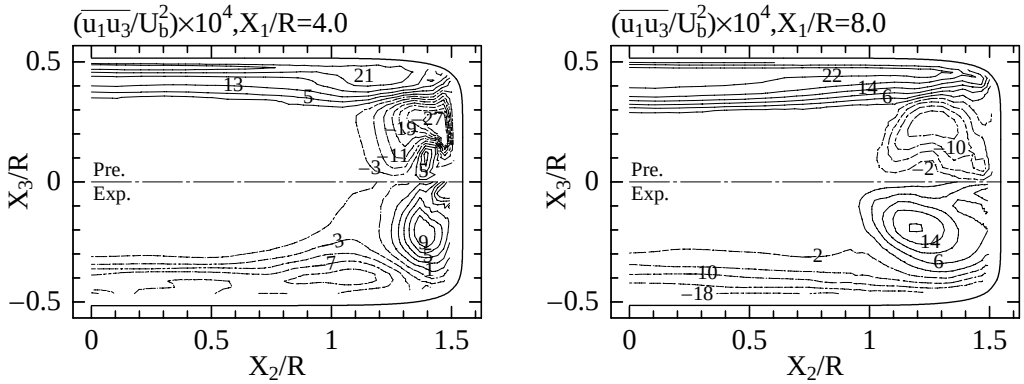

Figure 8. Comparison of shear stress $\overline{u_1 u_3}$

for contours of $X_1/R = 8.0$ about the midplane $X_3/R = 0$ in the vicinity of the duct sidewall. These distorted contours are caused by the pressure-driven secondary flow. The developments of secondary flow in the CR transition duct are predicted well by using the present method. Reasonable prediction of the secondary flow is indispensable to precisely predict the distorted contours of axial mean velocity and Reynolds stresses.

As for the normal component of Reynolds stresses, though the present method has a tendency to overestimate its value, characteristics features are reproduced without a great discrepancy. In addition, such tendency to overestimate Reynolds stresses is observed more clearly at $X_1/R = 4.0$ than at $X_1/R = 8.0$. The distributions of primary shear stresses are bound up with the gradient of streamwise velocity. The signs of shear stress $\overline{u_1 u_2}$ and $\overline{u_1 u_3}$ coincide with those of the primary rate of strains $\partial U_1/\partial X_2$ and $\partial U_1/\partial X_3$ deduced from contour plots of the streamwise velocity, respectively. The calculated results of shear stress are in good agreement with the experimental data.

ACKNOWLEDGMENT

The authors would like to express their appreciation to Dr. D.O. Davis (NASA Lewis Research Center) and Professor Gessner(University of Washington) for making, in magnetic form, experimental data for the CR transition duct available.

REFERENCES

Davis,D.O.,and Gessner,F.B.,1992,"Experimental investigation of turbulent flow through a circular-rectangular transition duct,"AIAA Journal, Vol.30, No.2, pp.367-375

Davis,D.O.,1991,"Experimental investigation of turbulent flow through a circular-to-rectangular transition duct," NASA TM105210

Gessner,F.B., and Eppich,H.M., 1981, "A new-wall pressure-strain model for turbulent corner flows,"Proc. 3rd. Symp. Turbulent Shear Flows, Vol.103, pp.445-455

Lien,F.S.,and Leschziner,M.A., 1993, "Computational modelling of 3D turbulent flow in S-diffuser and transition duct,"Engineering Turbulence Modelling and Experiments 2, pp.217-227

Launder,B.E.,Reece,G.J.,and Rodi,W.,1975,"Progress in the development of a Reynolds stress turbulence closure," J.Fluid Mech., Vol.68, pp.537-566

Leonard,B.P.,1979,"A stable and accurate convective modelling procedure based on quadratic upstream interpolation,"Comp. Meths. Appl. Mech. Eng., Vol.19, pp.59-98

Rodi,W.,1976,"A new algebraic relation for calculating the Reynolds stresses," Z.Angew. Math. Mech., Vol.56, pp.T219-T221

Sotiropoulos,F.,and Patel,V.C.,1994,"Prediction of turbulent flow through a transition duct using a second-moment closure,"AIAA Journal, Vol32, No.11, pp.2194-2204

Sugiyama,H.,Akiyama,M.,Matsumoto,M.,Hirata,M., and Ninomiya,N., 1993, "Numerical analysis of fully developed turbulent flow in a square duct with two facing roughened walls," Computational Fluid Dynamics JOURNAL, Vol.2, No.3, pp.319-338

Sugiyama,H., Akiyama,M., Yamanaka,Y., and Hirata, M., 1995 , "Numerical analysis of turbulent structure in a rectangular duct with sand ridges, "Computational Fluid Dynamics JOURNAL, Vol.4., No.1, pp.59-78